# A WIGGLE-MATCHED 297-YR TREE-RING OXYGEN ISOTOPE RECORD FROM THAILAND: INVESTIGATING THE ^{14}C OFFSET INDUCED BY AIR MASS TRANSPORT FROM THE INDIAN OCEAN

Masaki Sano[1]*[ORCID] • Nathsuda Pumijumnong[2] • Koji Fujita[1] • Masataka Hakozaki[3] • Fusa Miyake[4] • Takeshi Nakatsuka[1]

[1]Graduate School of Environmental Studies, Nagoya University, Nagoya, Japan
[2]Faculty of Environment and Resource Studies, Mahidol University, Thailand
[3]National Museum of Japanese History, Sakura, Japan
[4]Institute for Space-Earth Environmental Research, Nagoya University, Nagoya, Japan

**ABSTRACT.** Regional offsets from Northern Hemisphere radiocarbon (^{14}C) calibration curves are widely recognized for monsoon Asia and often hinder accurate ^{14}C dating. In this paper, we explore the possible linkage between summer monsoon intensity and ^{14}C offsets using tree-ring $\delta^{18}O$ and ^{14}C data from Thailand. We developed a 297-yr floating tree-ring $\delta^{18}O$ chronology comprising seven teak log-coffin samples from the Ban Rai rock shelter site, northwestern Thailand. The outermost ring of our chronology was estimated to date from 358–383 CE, within a 95.4% ($2\sigma$) probability range, based on a total of 10 ^{14}C measurements that were wiggle-matched against a mixed calibration curve evenly weighted from the IntCal20 and SHCal20 curves. Backward trajectory analysis showed that an intensified (weakened) summer monsoon detected in a modern tree-ring $\delta^{18}O$ chronology was most likely to be induced by increased (decreased) air mass transport from the tropical Indian Ocean, which is an area of intense upwelling where the ^{14}C concentration is lower than the atmospheric ^{14}C level. However, partly because of the limited sample size and dating uncertainty, the direct linkage between the tree-ring $\delta^{18}O$ series and ^{14}C records obtained from our teak log-coffin samples could not be statistically verified.

**KEYWORDS:** air mass pathway, ^{14}C offset, monsoon, teak, tree-ring $\delta^{18}O$, wiggle matching.

## INTRODUCTION

Over the last couple of decades, considerable effort has been devoted to developing substantially improved ^{14}C calibration curves that better reflect past atmospheric radiocarbon (^{14}C) concentrations, and this has led to the latest suite of calibration curves, including IntCal20, which is used for the calibration of Northern Hemisphere terrestrial samples (Reimer et al. 2020). Similarly, SHCal20 has been individually developed for the calibration of Southern Hemisphere terrestrial samples (Hogg et al. 2020). This is because ^{14}C data obtained from tree rings from the Southern Hemisphere are depleted relative to those from the Northern Hemisphere, and the degree of north–south hemispheric ^{14}C offset is not stable but varies temporally (e.g., McCormac et al. 1998; Hogg et al. 2002). Another important factor that contributes to the accuracy of ^{14}C dating is inter-hemispheric air mass mixing, which appears to be significant in tropical and a few subtropical regions influenced by monsoon circulations (Hua and Barbetti 2007). Moreover, the seasonal position of the tropical low-pressure belt (TLPB; Figure 1) associated with monsoon circulations is temporally and spatially variable (Ancapichún et al. 2021; Hua et al. 2022), indicating that the degree of north–south air mass mixing is also unstable. The entire period of the IntCal20 and SHCal20 calibration curves cannot be used to accurately date samples from regions influenced by the TLPB. Therefore, producing new calibration curves for these regions (e.g., the NH zone 3 or SH zone 3 defined by Hua et al. 2022) will be necessary if we wish to move toward more accurate ^{14}C dating.

---

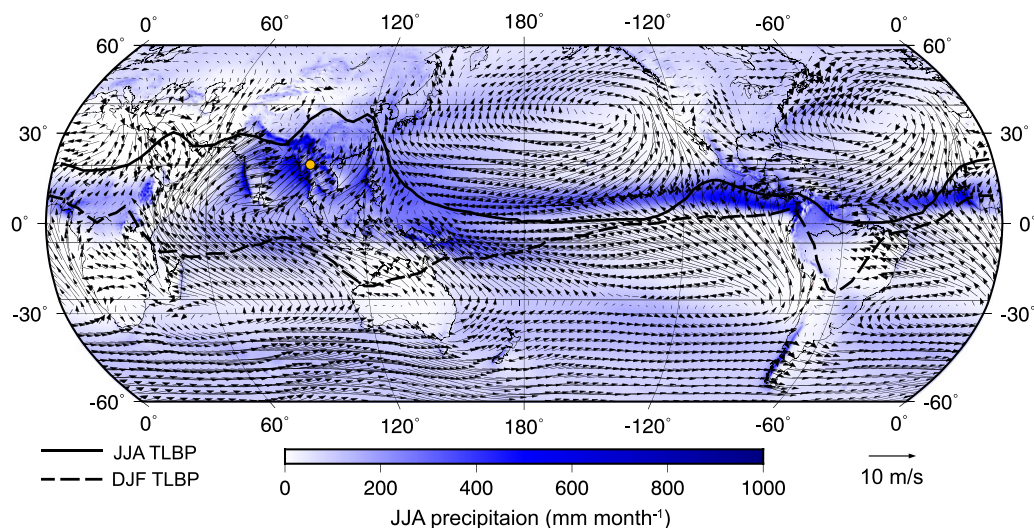*Corresponding author. Email: msano@nagoya-u.jp

CrossMark

Figure 1   Global map showing the location of our sampling site (orange circle) and climatological components. The long-term (1950–2019 CE) mean surface wind vectors and precipitation (mm month$^{-1}$) for the June–August period are represented by arrows and blue shading, respectively, and were derived from the ERA5 dataset (Hersbach et al. 2020). The mean positions of the TLPB during June–August (JJA: solid line) and December–February (DJF: dashed line) were derived from Hua et al. (2022) and are based on the NCEP/NCAR sea level pressure data. (Please see online version for color figures.)

Most tropical trees do not form annual growth rings owing to a general lack of climatic seasonality, making it difficult to obtain reliable dendrochronological dates. However, there are some regions with distinct wet and dry seasons induced by the seasonal driver of the monsoon. Northern Thailand is one such region, and tree-ring chronologies have been successfully established using two species of mountain pine (Buckley et al. 1995) and also teak (Pumijumnong et al. 1995; Buckley et al. 2007). A 448-yr chronology (1558–2005 CE) based on ring widths from teak is the longest tree-ring record yet produced from Thailand (Buckley et al. 2007). Extending this chronology further back is challenging, as the older teak trees have been almost entirely removed by logging. Fortunately, archaeological remains of wooden materials made of teak have been preserved in dry caves, and these are important at least for the development of a floating chronology (Pumijumnong and Wannasri 2015).

Pumijumnong et al. (2020) constructed a teak tree-ring $\delta^{18}O$ chronology for northwestern Thailand covering the period 1678–2015 CE. Compared with conventional dendrochronology based on ring widths, oxygen isotope ratios in tree rings are well correlated between different trees (e.g., Sano et al. 2012a, 2012b). Therefore, tree-ring $\delta^{18}O$ data can be used to robustly date a dataset with a limited number of tree-ring samples even if the ring width series cannot be cross-dated by conventional dendrochronological analysis (Loader et al. 2019; Sano et al. 2022). In addition, being controlled simply by two climatic parameters (i.e., the $\delta^{18}O$ of precipitation and relative humidity), tree-ring $\delta^{18}O$ can be used to precisely reconstruct past hydroclimatic variations, such as during the summer monsoon season in Southeast Asia (Sano et al. 2012b; Xu et al. 2013; Pumijumnong et al. 2020). Therefore, we used the climatic strength of tree-ring $\delta^{18}O$ to test whether tree-ring $\delta^{18}O$ can act as a proxy for inter-hemispheric air mass mixing. Based on radiocarbon preserved in tree rings from Thailand, Hua et al. (2004a, 2004b) proposed that northward movement (~30°N) of the intertropical

convergence zone (ITCZ) during boreal summer stimulates the incursion of air parcels originating in the Indian Ocean or the Southern Hemisphere. The supply of moisture from areas far from the tree-ring site is assumed to reflect an intensified summer monsoon that leads to wetter conditions, and these conditions are precisely recorded as a decrease in teak tree-ring $\delta^{18}$O preserved in Thailand (Pumijumnong et al. 2020). Collectively, an increase in the air mass flow from the tropical Indian Ocean, which is an area of intense upwelling with a lower $^{14}$C concentration than the atmospheric $^{14}$C level, could possibly be detectable using measurements of both tree-ring $^{14}$C and $\delta^{18}$O.

In the present study, we developed a 297-yr floating chronology using seven tree-ring $\delta^{18}$O series obtained from teak log-coffin samples from the Ban Rai rock shelter site, northwestern Thailand. The floating chronology was then anchored by wiggle-matching calibration. Based on earlier findings (Hua and Barbetti 2007), our wiggle matching was conducted using a mixed calibration curve evenly weighted from the IntCal20 and SHCal20 curves. Subsequently, the link between modern tree-ring $\delta^{18}$O (Pumijumnong et al. 2020) and air mass transport from the Indian Ocean was scrutinized using backward trajectory analysis. Finally, we explored the possible linkage between summer monsoon intensity and $^{14}$C offset from the SHCal20 curve using the tree-ring $\delta^{18}$O and $^{14}$C records.

## MATERIALS AND METHODS

### Study Site and Sampling

The tree-ring samples used for this study were collected from coffins, pillars, and beams at the Ban Rai rock shelter site (19°33′N, 98°11′E), which is located at an elevation of 793 m above sea level (asl) on a hillside in Mae Hong Son Province, northwestern Thailand (Figure 1). The rock shelter has a horseshoe-shaped south-facing opening, and is approximately 105 m wide by 142 m long (Pumijumnong and Wannasri 2015). The shelter is situated under an overhanging cliff, which is 30 m high and limits the direct influence of precipitation. Log coffins, resting on two or three pairs of pillars, were interred at the site, and a detailed description of the excavation can be found in Treerayapiwat (2005). All samples obtained from the shelter were made of teak (*Tectona grandis* L.), which produces annual growth rings, and increment cores or thin blocks were collected from the teak for tree-ring analysis.

### Tree-Ring Oxygen Isotope Data

Isotope analysis was carried out on a total of seven samples from seven different trees, each of which contained more than 100 rings. Cellulose was isolated directly from 1-mm-thick tree-ring laths (Xu et al. 2011; Kagawa et al. 2015). This method allows us to preserve the anatomical structure of the wood during the chemical treatment, facilitating the processing of hundreds of rings simultaneously. A modified protocol, which is based on the standard methodology (Green 1963; Loader et al. 1997), was used to isolate the cellulose from the whole wood. Each annual ring sample (120–250 µg) was then separated from adjacent rings in a cellulose lath using a razor blade and a microscope. The oxygen isotope ratios ($^{18}$O/$^{16}$O) in the cellulose samples were measured in an isotope ratio mass spectrometer (Delta V Advantage, Thermo Fisher Scientific) connected to a pyrolysis-type elemental analyzer (High Temperature Conversion Elemental Analyzer, Thermo Fisher Scientific) interfaced with a Conflo III (Thermo Fisher Scientific). The oxygen isotope ratios are reported as $\delta^{18}$O (‰), deviations relative to the international Vienna Standard Mean Ocean Water (VSMOW). The reproducibility of the repeatedly measured in-house standard material (Merck cellulose) was less than 0.2‰ (1σ).

To cross-check the reliability of pattern-matching among different samples, we also measured all of the annual growth rings to an accuracy of 0.01 mm using a TA Unislide measurement system (Velmex Inc.). As we found that the ring width variations were only weakly correlated among the seven samples, the ring width data previously recovered from the other seven samples at the same site (Pumijumnong and Wannasri 2015) were merged into the dataset and used for cross-dating. The previous ring width series have been statistically cross-dated using the COFECHA program (Holmes 1983). The cross-dated ring width series were then averaged to produce a local chronology (Pumijumnong and Wannasri 2015), against which our ring width chronology consisting of the seven samples was cross-dated by matching the ring width patterns.

## Chronology Development

Pattern matching of inter-annual $\delta^{18}O$ variations was conducted to assign relative years for every ring among the seven tree-ring $\delta^{18}O$ series produced in this study. Following the principle of cross-dating, correlation analysis using paired series from the seven series was carried out to identify the relative years showing the highest correlation coefficient. The strength of common variations among the seven series was evaluated by calculating the mean inter-series correlation (Rbar) and the expressed population signal (EPS), the latter being calculated using the number of samples and Rbar (Wigley et al. 1984). Some of our tree-ring $\delta^{18}O$ series showed long-term increasing trends with increasing tree age (Figure 2a). This was particularly significant with samples C58 and C59. However, others showed only a weak upward trend (P05 and C62) or no trend at all (C60, C12A, and C10). Based on statistical tests of isotope datasets with relatively high sample sizes, Duffy et al. (2019) and Büntgen et al. (2020) concluded that there are no age-related trends in tree-ring $\delta^{18}O$ series obtained from oak. More specifically, of 17 modern oak trees, 11 (6) showed increasing (decreasing) trends, 6 (1) of which were (was) statistically significant (Duffy et al. 2019). Similar to their study (Duffy et al. 2019), the proportion of series showing positive and negative trends in our tree-ring data turned out to be non-significant based on the binomial test. Although our data were not inconsistent with those findings (Duffy et al. 2019), the $\delta^{18}O$ values of C58 and C59 from the earlier period were shown to be markedly lower than those of the other samples. Some ecological and/or physiological factors that were unique to these two trees (C58 and C59) during their younger phase could be reflected in their $\delta^{18}O$ values. It is also plausible that the positive trend was partially induced by long-term climate variability, as four of the seven teak samples showed positive trends. However, a larger sample size will be needed to rigorously test whether teak tree-ring $\delta^{18}O$ in this region is modulated by aging. Following the usual procedure for tree-ring standardization (Fritts 1976), we detrended the series to remove this age-dependent long-term tendency, while at the same time attempting to retain decadal-scale variations related to hydroclimate. Specifically, each of the tree-ring series was individually detrended by fitting a straight line, and subsequently subtracted to produce anomalies from the fitted values. All of the detrended tree-ring $\delta^{18}O$ series were then averaged to build the final chronology.

Based on the relative dates determined from pattern matching of the tree-ring $\delta^{18}O$ data, we calculated the inter-series correlations between the ring width series to evaluate the robustness of the cross-dating. As the teak from the study region grows in closed forests, tree growth is significantly modulated by ecological interactions among neighboring trees. Additional data-adaptive detrending is therefore required to remove these ecological pulses, which are unique to
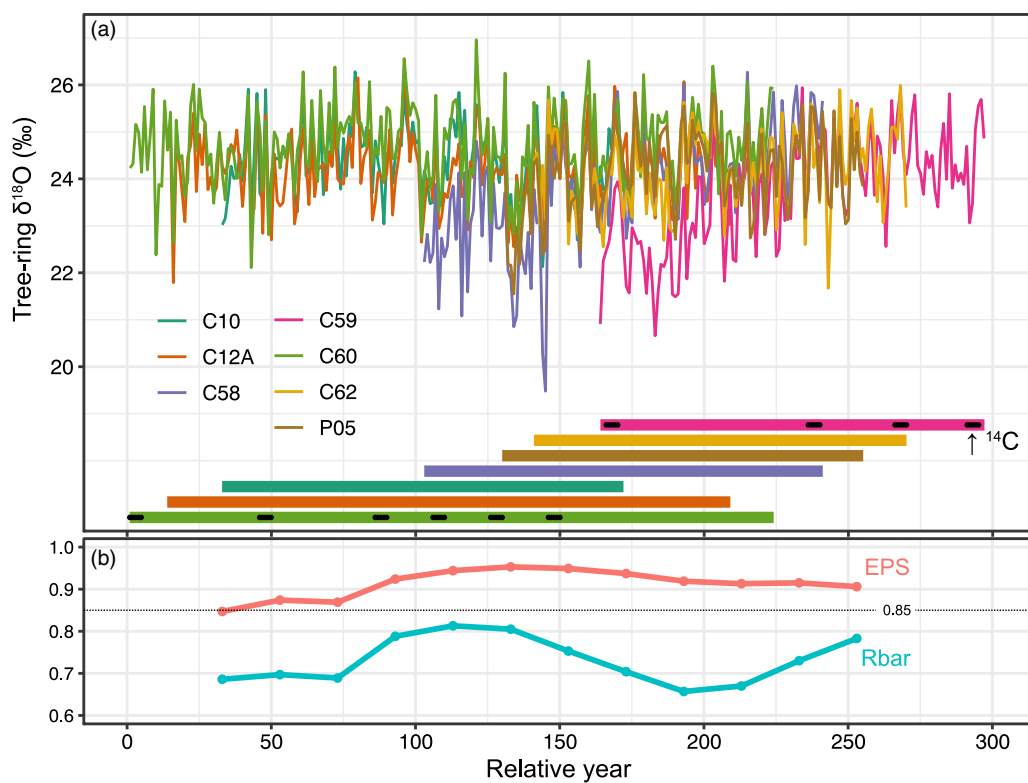
Figure 2 (a) Synchronized tree-ring $\delta^{18}O$ series from the seven teak samples and their time spans showing the 5-yr sequences used for the AMS $^{14}C$ measurements. The horizontal axis represents relative years, with the oldest ring corresponding to year 1. (b) The running Rbar (mean inter-series correlation) and EPS (expressed population signal) statistics calculated over 40 yr and lagged by 20 yr.

individual trees. To extract the high-frequency variability component from the raw data, we detrended the individual ring width series by fitting a cubic smoothing spline (Cook and Peters 1981) with a 50% variance reduction at 10 yr. Correlation tests were then performed using the detrended series for all possible pairs. In addition, each of the 60-yr segments extracted from the individual ring width series was correlated against a site chronology that was developed using all of the remaining samples (i.e., the leave-one-out principal). Our analysis was performed using the dendrochronology program library in R (dplR; Bunn 2008).

**Radiocarbon Measurements and Wiggle Matching**

Ten samples were selected for the $^{14}C$ measurements. Each $^{14}C$ sample consisted of five consecutive rings, and these relative years are listed in Table 1. The gaps between the $^{14}C$ measurements ranged from 20 to 70 yr. To avoid potential contamination in reusing the cellulose laths used for $\delta^{18}O$ analysis, cellulose was independently extracted from each of the whole wood samples consisting of only five rings for $^{14}C$ measurement. $^{14}C$ was measured in a compact accelerator mass spectrometer (National Electrostatics Corporation) at Paleo Lab Co., Ltd, Japan, and the analytical precision of the $^{14}C$ ages was 19–25 yr ($1\sigma$). Our sampling site is strongly influenced by the Asian monsoon, which is at least partially responsible for the air mass flow that originates in the Southern Hemisphere (Hua

Table 1   Sample description and ^{14}C results based on a mixed calibration curve evenly weighted from the IntCal20 and SHCal20 curves.

| No.* | Sample ID* | AMS lab ID | Relative year* (1 = oldest) | [14]C age (BP ± 1σ) | Calendar year (2σ) without wiggle matching | Calendar year (2σ) with wiggle matching |
|------|-----------|-----------|------------------------------|----------------------|---------------------------------------------|------------------------------------------|
| 1 | C60 | PLD-33799 | 1–5 | 1944 ± 21 | 26–198 CE | 64–89 CE |
| 2 | C60 | PLD-34053 | 46–50 | 1908 ± 21 | 78–209 CE | 109–134 CE |
| 3 | C60 | PLD-34054 | 86–90 | 1886 ± 21 | 119–224 CE | 149–174 CE |
| 4 | C60 | PLD-34055 | 106–110 | 1872 ± 20 | 125–230 CE | 169–194 CE |
| 5 | C60 | PLD-34056 | 126–130 | 1914 ± 20 | 76–206 CE | 189–214 CE |
| 6 | C60 | PLD-33800 | 146–150 | 1868 ± 25 | 124–238 CE | 209–234 CE |
| 7 | C59 | PLD-34057 | 166–170 | 1786 ± 20 | 235–343 CE | 229–254 CE |
| 8 | C59 | PLD-34058 | 236–240 | 1757 ± 20 | 249–365 CE | 299–324 CE |
| 9 | C59 | PLD-34059 | 266–270 | 1750 ± 19 | 250–376 CE | 329–354 CE |
| 10 | C59 | PLD-33801 | 291–295 | 1728 ± 22 | 254–410 CE | 354–379 CE |
| Wiggle-matched date: Relative year 297 (outermost ring) = 358–383 CE (2σ) | | | | | | |

*Correspond to those used in Figure 7.

and Barbetti 2007). Following a simple approach (Marsh et al. 2017, 2018; Hogg et al. 2020), we created an evenly weighted mixed curve that combined the IntCal20 and SHCal20 curves for the age calibration procedure, which was generated using the "Mix_curve" command in the OxCal online v4.4 program (Bronk Ramsey 2009). Based on the ^{14}C gap year data derived from dendrochronology, all of the ^{14}C data were wiggle-matched against the mixed calibration curve.

**Backward Trajectory Analysis**

We investigated the possible impact of air mass transport pathways on tree-ring $\delta^{18}O$ and ^{14}C concentration using the HYSPLIT model (Hybrid Single-Particle Lagrangian Integrated Trajectory) distributed by NOAA (National Oceanographic and Atmospheric Administration; Stein et al. 2015). We used the NCEP/NCAR reanalysis data, which have a 2.5° horizontal resolution and 6-hour frequency (Kalnay et al. 1996) and are already formatted for the HYSPLIT model. Six heights ranging from 0 to 2500 m above ground level (500-m steps) were set as starting points for this analysis. Twenty-day backward trajectories were calculated between 1950 and 2019 CE for the May–October period, which is the teak growing season in northwestern Thailand, as identified from the climatic response of modern tree-ring $\delta^{18}O$ (Pumijumnong et al. 2020). A total of 4416 trajectories [4 times (0000, 0600, 1200, and 1800 UTC) × 184 days × 6 heights] were eventually obtained for each year. The outputs of the trajectory calculations were recorded hourly at each of the six heights. All air parcels below 2500 m above ground level were counted at a resolution of 1° × 1° (latitude × longitude) and backwards in time until the 20th day was reached. The counts from every grid were then expressed as the probability distribution ($p$, %):

$$p_{x,y,d} = \frac{\sum_d c_{x,y,d}}{\sum_d \sum_y \sum_x c_{x,y,d}} \times 100 \tag{1}$$

where, $p_{x,y,d}$ and $c_{x,y,d}$ are the probability and count of the air parcels, respectively, in a grid cell at a given longitude ($x$, degrees) and latitude ($y$, degrees) for a given trajectory period ($d$, days). Similarly, the relative contributions of the air masses transported from the ocean were calculated by counting the air parcels that originated in the ocean over the 20 days. Based on a teak tree-ring $\delta^{18}O$ record (1678–2015 CE) from northwestern Thailand (Pumijumnong et al. 2020), the wettest and driest 5 yr were selected between 1950 and 2015 CE (see Supplementary Material). The mean state of the air mass pathways, and the difference between the wettest and driest 5 yr were then calculated to explore the land–ocean air mass flow contributions. In addition, we used the ERA5 reanalysis dataset (Hersbach et al. 2020) to calculate the composite anomalies of the wettest and driest 5 yr for precipitation and surface wind during the May–October period.

## RESULTS AND DISCUSSION

During the process of pattern matching based on our tree-ring $\delta^{18}O$ series, no missing rings were identified in the tree-ring samples. Our tree-ring $\delta^{18}O$ series derived from the seven samples showed significant inter-series correlations over the common period, as indicated by the running Rbar statistics that ranged from 0.66 to 0.81 (Figure 2). In addition, the running EPS statistics ranged from 0.85 to 0.95, which exceeds the generally accepted threshold value of 0.85. Similarly, all pairs of tree-ring $\delta^{18}O$ series with at least a 30-yr overlap showed significant correlations at $p < 0.001$ (Figure 3a). In contrast, the ring width series exhibited relatively weak correlations among the seven samples (Figure 3b). The mean inter-series correlation of ring width was 0.17, which is notably lower than the 0.42 derived from the teak samples from northwestern Thailand (Buckley et al. 2007). This is at least partially related to within-tree noise generated by uneven radial growth. Buckley et al. (2007) countered this problem by measuring multiple radii per stem to obtain the mean growth of the individual tree. Unfortunately, we could not follow their method because of the lack of cross-sectioned samples. Instead, we used the ring width series reported by Pumijumnong and Wannasri (2015). The ring width patterns were successfully cross-matched with those in our dataset. As shown in Figure 4, most of the 60-yr segments from individual ring width series showed significant correlations with a site chronology, which was developed using all of the remaining series (leave-one-out principle). We believe that the reliability of our dating results, based on tree-ring $\delta^{18}O$, is further supported by the ring width data. Overall, our tree-ring records (both $\delta^{18}O$ and ring width) can be consistently replicated. It should be noted, however, that the latest period covered by our tree-ring records is based on only one sample (C59). Thus, neither the $\delta^{18}O$ nor ring width series were replicated during that period, which corresponds to relative years of 271–297 for $\delta^{18}O$ (Figure 2) and 309–335 for ring width (Figure 4). Although this uncertainty remains, almost the entire period of our tree-ring $\delta^{18}O$ chronology can be used to provide robust estimates of mean tree-ring $\delta^{18}O$ in our study region.

As shown in Table 1, the 95.4% (2σ) probability range is 106–173 yr for the calendar years without wiggle matching. Our wiggle-matching calibration (Supplementary Figure 1) successfully narrows down this probability range to 26 yr, with the relative year 297 (outermost ring) corresponding to 358–383 CE (95.4% probability range). The mixed curve used for calibration works well when compared with the probability ranges of 30 yr from
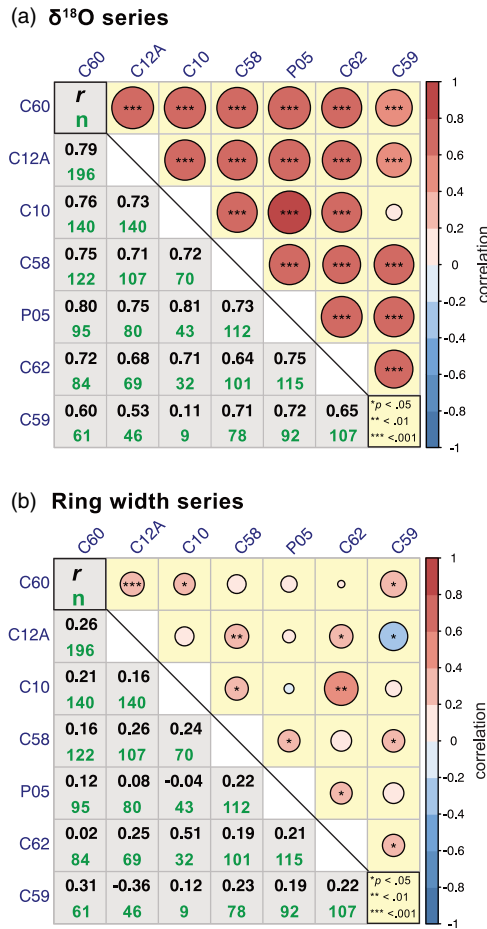
Figure 3   Correlation matrix for the (a) tree-ring δ¹⁸O series and (b) ring width series derived from the seven samples analyzed in this study. The raw series were individually standardized using a 10-yr smoothing spline function to extract high-frequency variations. The lower left of the matrix shows the correlation coefficient (*r*) together with the number of overlapping years (*n*), and the upper right shows the statistical significance with its correlation (corresponding to the size of the circle and color shading).

IntCal20 or 31 yr from SHCal20. This result is consistent with the shape of TLBP (Hua et al. 2022), and with Hua and Barbetti (2007), who estimated a 52% ± 13% contribution of Southern Hemisphere air masses to northern tropical and subtropical regions using atmospheric and tree-ring $^{14}$C data during the bomb-influenced period.

We then tested the possible link between modern tree-ring δ¹⁸O (Pumijumnong et al. 2020) and air mass transport from the Indian Ocean using backward trajectory analysis. The mean state of air mass pathways derived from our backward trajectory analysis is presented as the probability distribution of air masses arriving at the sampling site in summer (Figure 5a). Although some northeasterly winds from East Asia do blow across the site, a large proportion of the air masses that influence this site are transported from the Indian Ocean, including the Southern Hemisphere sector. As shown in Figure 5b, the difference in the probability distributions between the wettest and driest 5-yr composites clearly demonstrate
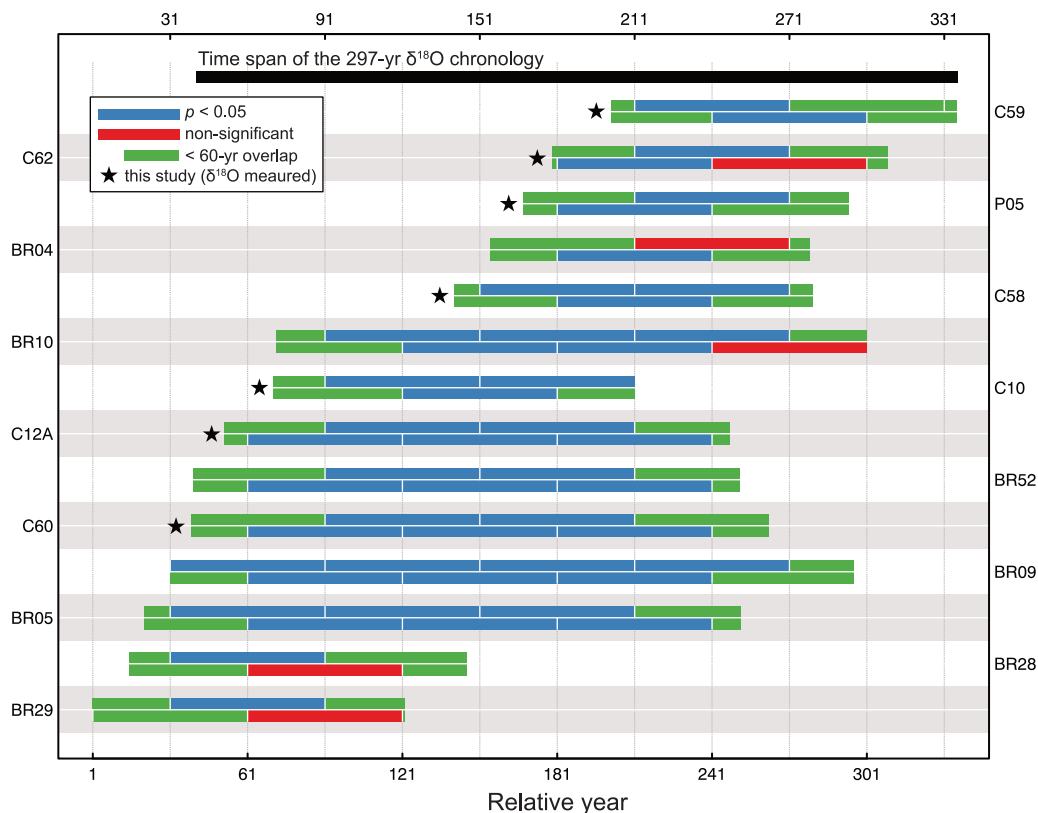
**Figure 4** Correlation tests of each ring width series against a site chronology, which was developed using all of the remaining series. Correlations were calculated for each 60-yr segment of the individual series, with segments lagged by 30 yr. Segments filled with blue, red, and green indicate significance at 5%, non-significance, and the end of samples with less than 60-yr overlaps, respectively. Stars represent samples with $\delta^{18}O$ data. The black bar represents the time span of the 297-yr tree-ring $\delta^{18}O$ chronology.

strengthened (weakened) air mass transport from the Indian Ocean (continental East Asia) in the wet years. Furthermore, a statistically significant difference in the relative contributions of air masses transported from the ocean was observed between the wettest and driest 5 yr ($t = 3.19$, degrees of freedom $= 8$, $p = 0.013$), indicating that intensification of the summer monsoon increases (decreases) air mass transport from the ocean (land). The normalized composite anomalies for precipitation and surface wind (10-m wind) from the ERA5 reanalysis data for the wettest and driest 5 yr (Figure 6) are also consistent with our findings. Specifically, the amount of precipitation, not only in our study region but also across wider areas of South and Southeast Asia, was accurately reflected in a tree-ring $\delta^{18}O$ record constructed from living teaks by Pumijumnong et al. (2020). The surface wind vectors indicate a strengthened (weakened) water supply from the ocean during the wettest (driest) 5 yr. Our findings based on the modern records indicate that an intensified (weakened) summer monsoon recorded as lower (higher) tree-ring $\delta^{18}O$ was most likely to be induced by increased (decreased) air mass transport from the tropical Indian Ocean, which is an area of intense upwelling where the $^{14}C$ concentration is lower than the atmospheric $^{14}C$ level.

Finally, we tested the possible linkage between summer monsoon intensity and $^{14}$C offset from the calibration curves using the $\delta^{18}$O and $^{14}$C data from our teak log-coffin samples. The 5-yr $\delta^{18}$O segments used for this analysis are shown in Figure 7a. The teak $^{14}$C age offsets from SHCal20 ($^{14}$C ages minus SHCal20) were compared with the corresponding 5-yr mean of the teak $\delta^{18}$O (Figure 7b). There was an inverse, but weak, association between the $^{14}$C age offsets and $\delta^{18}$O values. Although this is not inconsistent with our findings obtained from the modern data, the relationship was not statistically significant ($r = -0.30$, n $= 10$, $p = 0.40$), indicating that our hypothesis outlined above was not verified. The sample size of 10 seems to be too small to detect such a linkage, as there appears to be a slight difference between the IntCal20 and SHCal20 curves observed in Figure 7b. In addition, the output of this analysis is sensitive to the wiggle-matching uncertainty. The former can be improved by increasing the sample size, and the latter can be entirely overcome by using dendrochronologically dated samples. The sampling design of the $^{14}$C measurements is also important in this analysis. Specifically, calendar periods showing a significant $^{14}$C difference between the IntCal20 and SHCal20 curves (e.g., the period of sample No. 7 in Figure 7b) can be used to discriminate between the influence of air mass incursion from the northern and southern hemispheres. Therefore, the findings presented here are not sufficient to reject our hypothesis, but it is yet to be fully verified, and this will require the use of additional tree-ring $^{14}$C and $\delta^{18}$O data from regions significantly influenced by inter-hemispheric air mass mixing.

Our analysis presented here was based mainly on reanalysis datasets, and indeed the possible link between our tree-ring $\delta^{18}$O and $^{14}$C data was not statistically verified. Notwithstanding this limitation, the tree-ring $\delta^{18}$O data from the last several decades are consistent with our interpretation of air mass sources. This is because moisture source signals are related partly to regional $^{14}$C offsets and are well preserved in tree-ring $\delta^{18}$O data (Sano et al. 2020). Continued efforts toward developing a tree-ring dataset consisting of $\delta^{18}$O and $^{14}$C records will shed more light on the possible link between tree-ring $\delta^{18}$O and $^{14}$C.

## CONCLUSIONS

In this study, we developed a 297-yr tree-ring $\delta^{18}$O record from northwestern Thailand. Using 10 accelerator mass spectrometry (AMS) $^{14}$C measurements, we were able to date the last ring of our chronology to 358–383 CE (95.4% probability range) using a wiggle-matching calibration. Backward trajectory analysis indicates that an intensified (weakened) air mass flow from the tropical Indian Ocean is clearly recorded as lower (higher) tree-ring $\delta^{18}$O values. However, a direct linkage between tree-ring $\delta^{18}$O and $^{14}$C records from teak log-coffin samples could not be demonstrated.
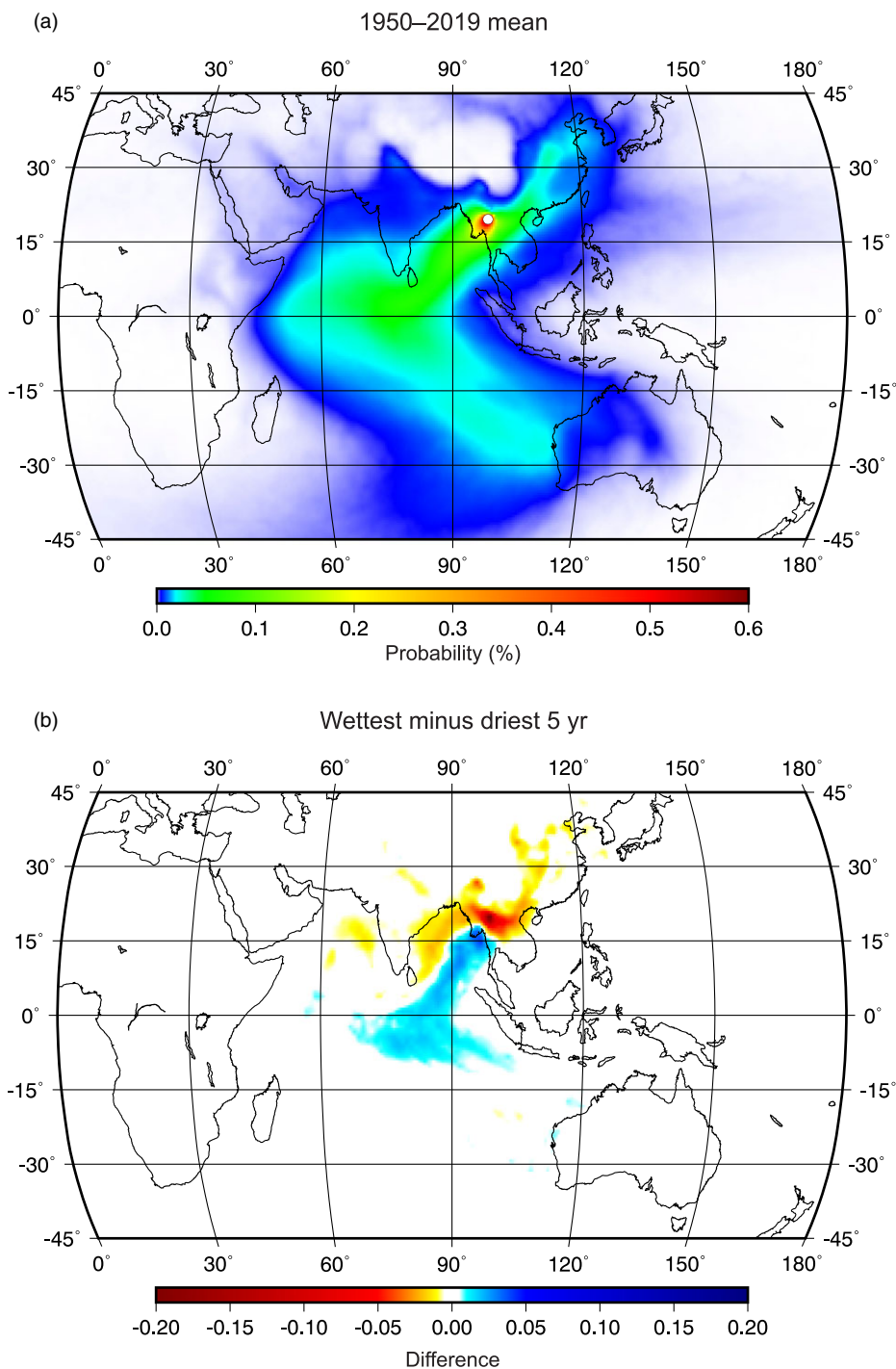
## ACKNOWLEDGMENTS

Figure 5 (a) Probability distribution of air mass arriving at the sampling site (open circle) for the May–October period derived from backward trajectory analysis between 1950 and 2019 CE. (b) Difference in probability distributions between the wettest and driest 5-yr composites.
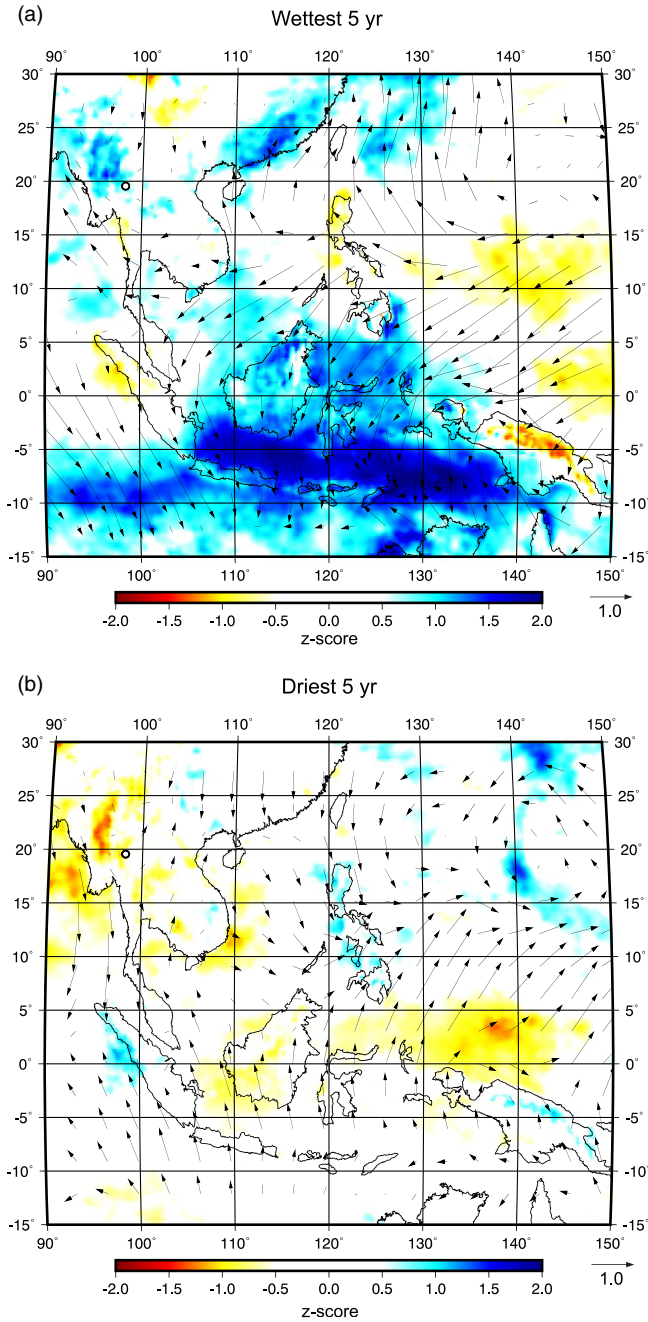
Figure 6 Normalized May–October composite anomalies of precipitation (color shading) and surface wind (arrows) for the (a) wettest and (b) driest 5 yr between 1950 and 2019. Open circle indicates our sampling site. Global-scale composite anomalies are presented in Supplementary Figure 2.
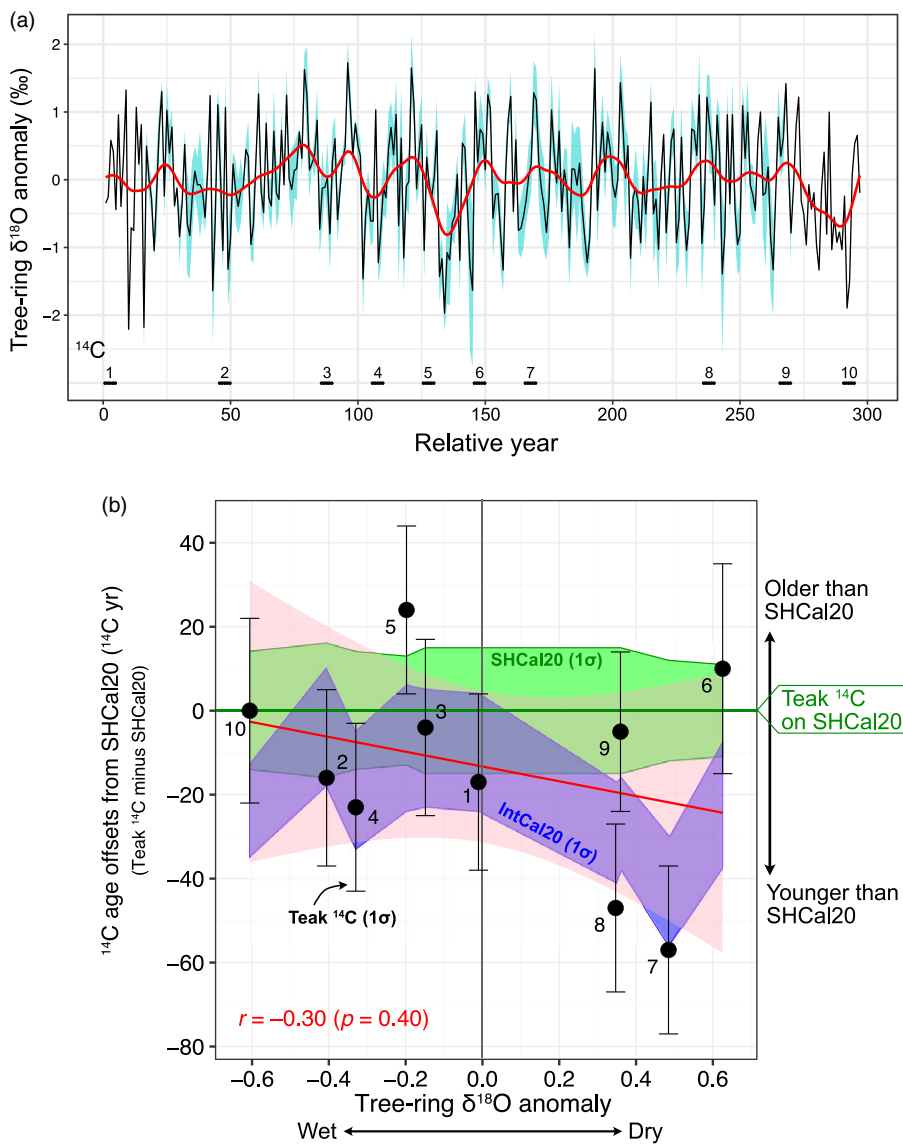
Figure 7 (a) The 297-yr tree-ring $\delta^{18}O$ chronology developed by averaging the seven detrended series. Blue shading and the red line represent ±1 standard deviation and 20-yr splined values, respectively. The 5-yr sequences used for $^{14}C$ measurements are marked with black bars. (b) Comparison between 5-yr mean tree-ring $\delta^{18}O$ anomaly and $^{14}C$ age offsets from the SHCal20 calibration curve (teak $^{14}C$ minus SHCal20). Error bars represent teak $^{14}C$ analytical precision (1σ). Green and blue shading indicate uncertainty (1σ) for SHCal20 (i.e., SHCal20 minus SHCal20) and IntCal20 (i.e., IntCal20 minus SHCal20), respectively. Pink shading represents the 95% confidence interval of the linear regression, in which the negative trend is not statistically significant. The individual $^{14}C$ and $\delta^{18}O$ data used for (a) and (b) are linked by the numbers (1–10) shown in both plots.

## DECLARATION OF COMPETING INTERESTS

The authors declare no conflicts of interest.

## SUPPLEMENTARY MATERIAL

To view supplementary material for this article, please visit https://doi.org/10.1017/RDC.2023.14

## REFERENCES

Ancapichún S, De Pol-Holz R, Christie DA, Santos GM, Collado-Fabbri S, Garreaud R, Lambert F, Orfanoz-Cheuquelaf A, Rojas M, Southon J, Turnbull JC, Creasman PP. 2021. Radiocarbon bomb-peak signal in tree-rings from the tropical Andes register low latitude atmospheric dynamics in the Southern Hemisphere. Science of the Total Environment 774:145126.

Bronk Ramsey C. 2009. Bayesian analysis of radiocarbon dates. Radiocarbon 51:337–360.

Buckley BM, Barbetti M, Watanasak M, D'Arrigo R, Boonchirdchoo S, Sarutanon S. 1995. Dendrochronological investigations in Thailand. IAWA Journal 16:393–409.

Buckley BM, Palakit K, Duangsathaporn K, Sanguantham P, Prasomsin P. 2007. Decadal scale droughts over northwestern Thailand over the past 448 years: links to the tropical Pacific and Indian Ocean sectors. Climate Dynamics 29:63–71.

Bunn AG. 2008. A dendrochronology program library in R (dplR). Dendrochronologia 26:115–124.

Büntgen U, Kolář T, Rybníček M, Koňasová E, Trnka M, Ač A, Krusic PJ, Esper J, Treydte K, Reinig F, Kirdyanov A, Herzig F, Urban O. 2020. No age trends in oak stable isotopes. Paleoceanography and Paleoclimatology 35: e2019PA003831.

Cook ER, Peters K. 1981. The smoothing spline: a new approach to standardizing forest interior tree-ring width series for dendroclimatic studies. Tree-Ring Bulletin 41:45–53.

Duffy JE, McCarroll D, Loader NJ, Young GHF, Davies D, Miles D, Bronk Ramsey C. 2019. Absence of age-related trends in stable oxygen isotope ratios from oak tree rings. Global Biogeochemical Cycles 33:841–848.

Fritts HC. 1976. Tree rings and climate. New York: Academic Press.

Green JW. 1963. Wood cellulose. In: Whistler RL, editor. Methods in carbohydrate chemistry. New York: Academic Press. p. 9–21.

Hersbach H, Bell B, Berrisford P, Hirahara S, Horányi A, Muñoz-Sabater J, Nicolas J, Peubey C, Radu R, Schepers D, et al. 2020. The ERA5 global reanalysis. Quarterly Journal of the Royal Meteorological Society 146:1999–2049.

Hogg AG, Heaton TJ, Hua Q, Palmer JG, Turney CSM, Southon J, Bayliss A, Blackwell PG, Boswijk G, Bronk Ramsey C, Pearson C, Petchey F, Reimer P, Reimer R, Wacker L. 2020. SHCal20 Southern Hemisphere calibration, 0–55,000 years cal BP. Radiocarbon 62:759–778.

Hogg AG, McCormac FG, Higham TFG, Reimer PJ, Baillie MGL, Palmer JG. 2002. High-precision radiocarbon measurements of contemporaneous tree-ring dated wood from the British Isles and New Zealand: AD 1850–950. Radiocarbon 44:633–640.

Holmes RL. 1983. Computer-assisted quality control in tree-ring dating and measurement. Tree-ring Bulletin 43:69–78.

Hua Q, Barbetti M. 2007. Influence of atmospheric circulation on regional $^{14}CO_2$ differences. Journal of Geophysical Research: Atmospheres 112, D19102. doi: 10.1029/2006JD007898.

Hua Q, Barbetti M, Zoppi U. 2004a. Radiocarbon in annual tree rings from Thailand during the pre-bomb period, AD 1938–1954. Radiocarbon 46:925–932.

Hua Q, Barbetti M, Zoppi U, Fink D, Watanasak M, Jacobsen GE. 2004b. Radiocarbon in tropical tree rings during the Little Ice Age. Nuclear Instruments and Methods in Physics Research Section B: Beam Interactions with Materials and Atoms 223–224:489–494.

Hua Q, Turnbull JC, Santos GM, Rakowski AZ, Ancapichún S, De Pol-Holz R, Hammer S, Lehman SJ, Levin I, Miller JB, Palmer JG, Turney CSM. 2022. Atmospheric radiocarbon for the period 1950–2019. Radiocarbon 64:723–745.

Kagawa A, Sano M, Nakatsuka T, Ikeda T, Kubo S. 2015. An optimized method for stable isotope analysis of tree rings by extracting cellulose directly from cross-sectional laths. Chemical Geology 393–394:16–25.

Kalnay E, Kanamitsu M, Kistler R, Collins W, Deaven D, Gandin L, Iredell M, Saha S, White G, Woollen J, et al. 1996. The NCEP/NCAR 40-year reanalysis project. Bulletin of the American Meteorological Society 77:437–471.

Loader NJ, Mccarroll D, Miles D, Young GHF, Davies D, Ramsey CB. 2019. Tree ring dating using oxygen isotopes: a master chronology for central England. Journal of Quaternary Science 34:475–490.

Loader NJ, Robertson I, Barker AC, Switsur VR, Waterhouse JS. 1997. An improved technique for the batch processing of small wholewood samples to α-cellulose. Chemical Geology 136: 313–317.

Marsh EJ, Bruno MC, Fritz SC, Baker P, Capriles JM, Hastorf CA. 2018. IntCal, SHCal, or a Mixed Curve? Choosing a $^{14}$C calibration curve for archaeological and paleoenvironmental records from tropical South America. Radiocarbon 60:925–940.

Marsh EJ, Kidd R, Ogburn D, Durán V. 2017. Dating the expansion of the Inca Empire: Bayesian models from Ecuador and Argentina. Radiocarbon 59:117–140.

McCormac FG, Hogg AG, Higham TFG, Lynch-Stieglitz J, Broecker WS, Baillie MGL, Palmer J, Xiong L, Pilcher JR, Brown D, Hoper ST. 1998. Temporal variation in the interhemispheric $^{14}$C offset. Geophysical Research Letters 25:1321–1324.

Pumijumnong N, Bräuning A, Sano M, Nakatsuka T, Muangsong C, Buajan S. 2020. A 338-year tree-ring oxygen isotope record from Thai teak captures the variations in the Asian summer monsoon system. Scientific Reports 10:8966.

Pumijumnong N, Eckstein D, Sass U. 1995. Tree-ring research on Tectona grandis in northern Thailand. IAWA Journal 16:385–392.

Pumijumnong N, Wannasri S. 2015. Teak log coffins in northwest Thailand: dated by dendrochronology and $^{14}$C-wiggle matching. Applied Environmental Research 37:1–16.

Reimer PJ, Austin WEN, Bard E, Bayliss A, Blackwell PG, Bronk Ramsey C, Butzin M, Cheng H, Edwards RL, Friedrich M, et al. 2020. The IntCal20 Northern Hemisphere radiocarbon age calibration curve (0–55 cal kBP). Radiocarbon 62:725–757.

Sano M, Li Z, Murakami Y, Jinno M, Ura Y, Kaneda A, Nakatsuka T. 2022. Tree ring oxygen isotope dating of wood recovered from a canal in the ancient capital of Japan. Journal of Archaeological Science: Reports 45:103626.

Sano M, Ramesh R, Sheshshayee M, Sukumar R. 2012a. Increasing aridity over the past 223 years in the Nepal Himalaya inferred from a tree-ring $\delta^{18}$O chronology. The Holocene 22:809–817.

Sano M, Xu C, Dimri AP, Ramesh R. 2020. Summer monsoon variability in the Himalaya over recent centuries. In: Dimri AP, Bookhagen B, Stoffel M, Yasunari T, editors. Himalayan weather and climate and their impact on the environment. Cham: Springer International Publishing. p. 261–280.

Sano M, Xu C, Nakatsuka T. 2012b. A 300-year Vietnam hydroclimate and ENSO variability record reconstructed from tree ring $\delta^{18}$O. Journal of Geophysical Research: Atmospheres 117, D12115. doi: 10.1029/2012JD017749.

Stein AF, Draxler RR, Rolph GD, Stunder BJB, Cohen MD, Ngan F. 2015. NOAA's HYSPLIT atmospheric transport and dispersion modeling system. Bulletin of the American Meteorological Society 96:2059–2077.

Treerayapiwat C. 2005. Patterns of habitation and burial activity in the Ban Rai rock shelter, northwestern Thailand. Asian Perspectives 44:231–245.

Wigley TML, Briffa KR, Jones PD. 1984. On the average value of correlated time series, with applications in dendroclimatology and hydrometeorology. Journal of Climate and Applied Meteorology 23:201–213.

Xu C, Sano M, Nakatsuka T. 2013. A 400-year record of hydroclimate variability and local ENSO history in northern Southeast Asia inferred from tree-ring $\delta^{18}$O. Palaeogeography, Palaeoclimatology, Palaeoecology 386:588–598.

Xu C, Sano M, Nakatsuka T. 2011. Tree ring cellulose $\delta^{18}$O of *Fokienia hodginsii* in northern Laos: a promising proxy to reconstruct ENSO? Journal of Geophysical Research 116, D24109. doi: 10.1029/2011JD016694.

**Supplementary Material**

Selection of the wettest and driest five years from a teak tree ring $\delta^{18}O$ record between 1950 and 2015 CE (Pumijumnong et al. 2020).

The tree ring $\delta^{18}O$ data between 1950 and 2015 CE were normalized to have a mean of 0 and a unit variance (converted to z-score). The wettest and driest five years were then selected and are shown below. Note that tree ring $\delta^{18}O$ is inversely correlated with the amount of precipitation.

Wettest five years

| Rank | Year | $\delta^{18}O$ (‰) | Z-score |
|------|------|---------------------|---------|
| 1st | 1973 | 22.60 | –2.52 |
| 2nd | 1975 | 22.86 | –2.19 |
| 3rd | 1970 | 23.02 | –1.99 |
| 4th | 2010 | 23.32 | –1.61 |
| 5th | 1959 | 23.50 | –1.39 |

Driest five years

| Rank | Year | $\delta^{18}O$ (‰) | Z-score |
|------|------|---------------------|---------|
| 1st | 2015 | 26.90 | 2.90 |
| 2nd | 2014 | 26.21 | 2.03 |
| 3rd | 1986 | 26.17 | 1.98 |
| 4th | 2012 | 26.10 | 1.90 |
| 5th | 1979 | 25.90 | 1.64 |

Pumijumnong N, Bräuning A, Sano M, Nakatsuka T, Muangsong C, Buajan S. 2020. A 338-year tree-ring oxygen isotope record from Thai teak captures the variations in the Asian summer monsoon system. Scientific Reports 10:8966.
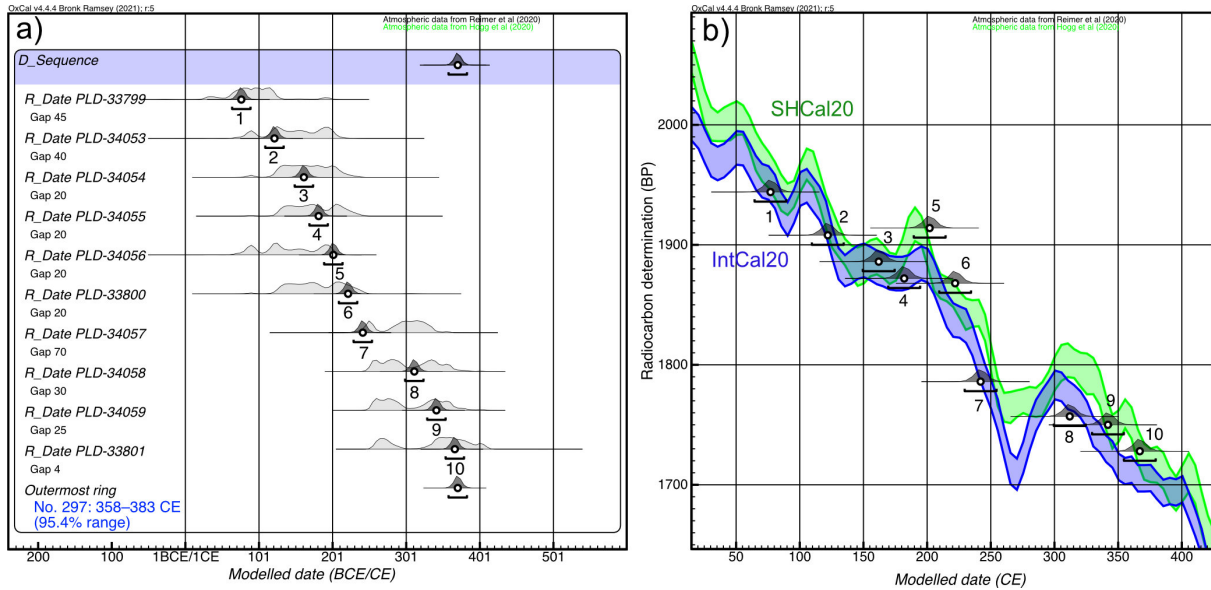
**Supplementary Figure 1.** (a) Radiocarbon dates based on a mixed calibration curve evenly weighted from the IntCal20 and SHCal20 curves. Probability distribution of the calibration without wiggle matching (light gray) and wiggle-matched model (dark gray, with 95.4% probability range at the bottom) are shown. The outermost ring (Relative year 297) falls in the range of 358–383 CE (95.4% probability) based on the wiggle-matching calibration. (b) The wiggle-matched dates on the IntCal20 and SHCal20 curves with 95.4% probability range (26-year bar) at the bottom.
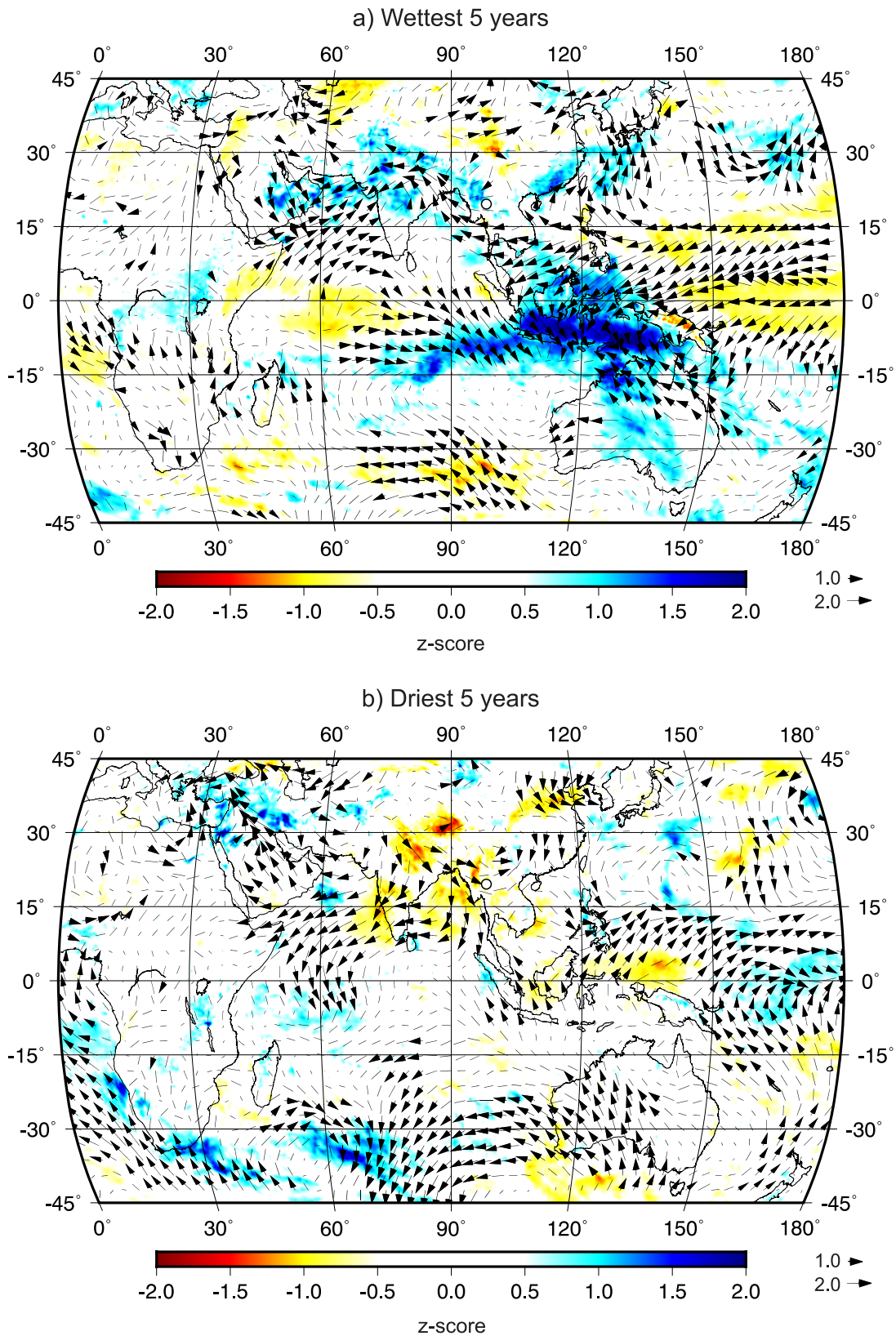
**Supplementary Figure 2.** Normalized May–October composite anomalies of global precipitation (color shading) and surface wind (arrows) for the (a) wettest and (b) driest five years between 1950 and 2019. Open circle indicates our sampling site (see Figure. 6 for regional-scale plots).